Journal of Neural Engineering

OPEN ACCESS

RECEIVED
2 April 2025

REVISED
31 October 2025

ACCEPTED FOR PUBLICATION
10 November 2025

PUBLISHED
19 November 2025

PAPER

A computational framework combining neuronal dynamics and evolutionary game theory for network-level synaptic interactions

Fabio Poggio[1], **Martina Brofiga**[1,2], **Cecilia De Vicariis**[1], **Vittorio Sanguineti**[1] and **Paolo Massobrio**[1,3,*]

[1] Department of Informatics, Bioengineering, Robotics, and Systems Engineering (DIBRIS), University of Genova, Genova, Italy
[2] Neurofacility, Istituto Italiano di Tecnologia (IIT), Genova, Italy
[3] National Institute for Nuclear Physics (INFN), Genova, Italy
[*] Author to whom any correspondence should be addressed.

E-mail: paolo.massobrio@unige.it

Keywords: evolutionary game theory, Hindmarsh–Rose, estimation method, neuronal networks

Supplementary material for this article is available online

Abstract

Objective. In this study, we present a novel computational framework that combines the Hindmarsh–Rose (HR) neuronal model with evolutionary game theory on networks to simulate and interpret synaptic-level interactions within neuronal populations. Our approach preserves the features of the HR model—capable of generating both spiking and bursting dynamics—while integrating game-theoretic principles that govern the balance between emulative and non-emulative behaviors across neurons. *Approach.* Neurons were modeled as strategic agents whose interactions evolve according to game-theoretic principles, allowing us to capture emergent network dynamics beyond classical electrophysiological analyses. A key innovation of our work is the formulation of a parameter estimation method based on adaptive observers, which enables the recovery of game-theoretic parameters solely from partial state observations. The proposed framework is validated through numerical simulations, demonstrating its ability to recover hidden parameters and accurately predict system behavior under diverse conditions. *Main results.* By applying the devised approach to synthetic datasets mimicking real electrophysiological recordings, we highlight its applicability in distinguishing neuronal populations based on their strategic interactions. In this context, the model is shown to faithfully reproduce both spiking and bursting behaviors, capturing the diverse electrophysiological patterns observed in *in vitro* experimental settings. Furthermore, we explore the potential of this model in experimental data analysis by suggesting that the estimated parameters may serve as discriminative markers for different neuronal types and structural characteristics. *Significance.* The integration of dynamical systems theory, game-theoretic modeling, and adaptive estimation provides a robust quantitative tool for investigating complex neuronal network dynamics. Our results quantitatively demonstrate the scalability and accuracy of the method in parameter estimation, reinforcing its value for systematic analysis of synaptic interactions and advancing our understanding of neuronal network dynamics.

1. Introduction

The investigation of the brain is one of the most intricate challenges of modern sciences. Despite its fundamental importance, our understanding of the brain remains limited, mainly due to its complexity, which stems from many factors, notably the huge number of neurons (more than 80 billion) and synaptic connections (more than 10^{20}). Furthermore, the brain's organization is complicated by the diversity among neurons, varying across different brain regions (e.g. cortex, hippocampus, thalamus), each with its distinct structure and function. Even within a specific brain region, individual neurons exhibit diverse functional behaviors (e.g. excitation vs. inhibition), influenced by their unique

morphological characteristics and their intricate network of synaptic connections. Addressing the challenges inherent in brain research demands a multidisciplinary approach, integrating expertise like biology, mathematics, electronics, physics, and computer science. In a reductionist approach, a possible method of investigation makes use of *in vitro* models, including cultures of dissociated neurons [1], neuronal slices [2], and brain organoids [3]. However, these models cannot be completely informative as some variables and parameters are not experimentally observable and measurable—for instance, the synaptic weights, which quantify the strength of the connection between two neurons, or the temporal evolution of ionic fluxes underlying membrane potential dynamics. They need support from mathematical and computational tools capable of explaining some experimental outcomes (especially the ones involving hidden mechanisms). Within this framework, *in silico* models assume a pivotal role, preceding the *in vitro* study, thereby complementing it. In the context of *in silico* models of a neuronal network, there are primarily two issues to address: i) modeling the single-neuron dynamics; ii) modeling the types of interactions among the neurons defining the network [4, 5]. Regarding the first issue, the electrophysiological activity can be simulated using models with a different degree of biological plausibility, (i.e. their ability to accurately represent the biophysical features of a real neuron), that influence the computational load for their simulation [6–8]. If conductance-based models (whose Hodgkin and Huxley one is the precursor [8]) take into account single-channel kinetics, the family of the integrate-and-fire neurons [9] completely neglect such sub-cellular level of detail, resulting a more phenomenological approach. A good trade-off is represented by the Hindmarsh–Rose (HR) model [7], a three-state system able to mimic both spiking and bursting regimes of activity, keeping the shape of the action potentials. Inherently, Hodgkin and Huxley model (containing only sodium and potassium voltage-dependent channels) is not able to reproduce bursting dynamics, except for the inclusion of persistent voltage-dependent sodium channels and/or potassium calcium dependent channels. However, the computational load grows dramatically. Although HR model is essentially a mathematical formalism without considering the biological component of the ionic channels, results a valid choice for the aim of this work. The second issue is the simulated connectivity which is typically modeled in terms of graph theory [10] to map the physiological interactions (synapses) among neurons. This formalism allows for the utilization of mathematical tools derived from graph theory (e.g. node degree, cluster coefficient, average path length, small-world indices, etc.) to provide a mathematical description of the network's connectivity [11]. Synapses can be described with bio-inspired models which allows to take into account the cascades of presynaptic (e.g. synthesis and release of neurotransmitters) and post-synaptic events (e.g. binding to receptors, recycle of neurotransmitters). In addition, these models are easily tailored for the type of synapse (excitatory vs inhibitory; ionotropic vs metabotropic). However, reductionist approaches can be also considered by means of linear combination of exponential kernels to describe the rise and decay phases of the synaptic currents. Finally, it is worth to mention that in the last years hybrid synapses—particularly in neuromorphic hardware and memristive systems—are also a relevant alternative [12]. Aware of the strategies for neuronal and synaptic modeling, in this work, we followed a complementary approach to describe the interaction between nodes in a network by means of the Game Theory (GT). In its original meaning, GT describes strategic interactions among individuals, where the reward of each player depends on both its own and other players' decisions [13]. The use of GT to describe the interaction of multiple agents is notable as during the years this approach has found successful applications in diverse fields, including economics [14], political science [15], biology [16], cooperation theory [17], as well as in modeling communication and interplay among different neuronal brain areas [18]. However, while GT focuses on static interactions driven by self-interest, it lacks describing more complex and dynamic behaviors observed in evolving systems [19]. To overcome these limits, evolutionary game theory (EGT) extends GT principles to evolving populations, emphasizing the dynamics of strategy change [20]. EGT is a powerful framework to understand the evolution of strategies within a population over time; yet, it remains constrained to population-level dynamics, offering no insight into the behavior of individual nodes or their local interactions. To overcome this further limitation, EGT has been extended to networked systems [21]. This approach, known as evolutionary games on networks (EGN), enables a more detailed analysis of how local interactions influence the collective behavior of the system [22]. In 2017, Madeo and coworkers successfully applied EGN to functional magnetic resonance imaging (fMRI) signals, leading to the formulation of the evolutionary games for brain networks (EGN-B), which demonstrated its ability to capture interregional brain dynamics, exploiting the balance between emulative and non-emulative components among cerebral regions [18]. The authors found that emulative behaviors occur when two nodes (i.e. brain regions) activate at relatively close time intervals, indicating synchronized dynamics. In contrast, non-emulative dynamics arise when one node activates while the other remains

inactive, and vice versa, reflecting an opposite pattern of interaction. With the formalism of the game theory, Madeo and coworkers represented each brain region as a 'player' engaging in strategic interactions influenced by its neighbors within a network. The dynamics are governed by the replicator equation, where the activation level of a region represents its real-time functional involvement, determined by its intrinsic tendencies towards activation and inhibition. By simulating these interactions, the model predicted low-frequency oscillatory behaviors resembling functional connectivity dynamics observed in resting-state fMRI data. Additionally, EGN-B demonstrated the capacity to approximate fMRI time series and to predict the impact of network lesions, underscoring its potential as a framework for understanding spontaneous brain activity and its alterations in pathological states.

In this work, we aim at providing a computational model that not only offers novel connectivity interpretation based on EGN in HR neuronal networks but also introduces an estimation method for parameter adaptation. The use of the EGN to mimic and explain the interaction at the synaptic level (microscopic scale) implies that the game theory parameters describing the relationships among neurons carry distinct information from that derived in other studies where connectivity is simulated using other methods [23, 24]. Our work proves the proposed model is able to preserve the fundamental principles of EGN, balancing emulation and non-emulation dynamics among different nodes (neurons), while maintaining the typical characteristics of the HR model, which allows the generation of both spinking and bursting dynamics. The setting up of the EGN parameters was performed by developing an estimation method based on the concept of adaptive observers [25]. This approach allows the estimation of both the state and the parameters of the model from the sole observation of the membrane potential of the neuron. Our findings prove the efficiency of both the model and the estimation method, even when applied to medium-scale neuronal networks. Finally, we proved how the simulation of the strategies predicted by the game theory recreates connectivity pathways resembling the small-world characteristics experimentally observed in *in vitro* cortical networks coupled to multi-electrode arrays (MEAs). To increase the versatility of the proposed model, we also introduced into the HR model an additional state equation to mimic the extracellular potential, i.e. the experimental signal of *in vitro* recordings, showing that the estimation process of EGT parameter remains effective even when the only observable variable is the extracellular membrane potential.

2. Materials and methods

2.1. HR neuronal model

In the present work, we utilized the HR model to simulate the emergent dynamics among synaptically connected neurons. The HR model allows for the mimicking of diverse electrophysiological dynamics exhibited by neurons, ranging from single action potentials (spikes) to oscillatory bursting activities [26]. For this reason, it can be considered a valuable tool for investigating various patterns of electrophysiological activity exhibited by real neurons. Mathematically, it is defined by the system of three differential equations reported in (1),

$$\begin{cases} \dot{x}(t) = y(t) - x^3(t) + bx^2(t) - z(t) + I \\ \dot{y}(t) = 1 - 5x^2(t) - y(t) \\ \dot{z}(t) = \mu(s(x(t) - x_r) - z(t)) \end{cases} \quad (1)$$

where state variable $x(t)$ describes the membrane potential of the neuron; state $y(t)$ accounts for the gating kinetics of the sodium and potassium channels; and $z(t)$ is a 'slow' state variable (related to the calcium dynamics) that supports the bursting behavior of a neuron.

The model has five additional parameters, namely b, μ, s, and x_r each playing a distinct role in shaping the system's behavior. Parameter b finely tunes the second-order contribution of $x(t)$. Different values of this parameter may lead to either spiking or bursting activity. Parameter μ modulates the amplitude of variation of $z(t)$ at each system evolution step, directly influencing the firing rate of the activity generated by the model. Parameter s controls the adaptation behavior of the neuron, with lower values (e.g. $s = 1$) resulting in constant spiking, and higher values (e.g. $s = 4$) leading to subthreshold overshoot and potential oscillations. Lastly, x_r represents the neuron's resting potential. Additionally, the model includes an exogenous input variable, I, which represents the input current contribution from other neurons of the network, or an external input current used to depolarize or hyperpolarize the neuron. For instance, Chen and co-workers demonstrated that by modulating the amplitude of the constant current input, a wide range of behaviors spanning from spiking, bursting up to chaotic dynamics can be achieved [27].

2.2. EGT

In 2017, Madeo and colleagues devised a mathematical model based on an extension of the EGT on brain networks (EGN-B), aimed to interpret the observed whole-brain resting state dynamics—evaluated in terms of blood-oxygen-level-dependent fMRI—by

means of the formalism of the interaction of multiple 'agents' (one per functional brain region).

Our working hypothesis posits that the interplay between brain areas described in [18] can be also applied at individual neuron level, considering local small/medium-scale neuronal networks. In this way, each neuron is modeled as an agent that must choose between two actions at each time instant: to become active (A) or to stay inactive (I). These actions are associated with different payoffs (2*a*) and (2*b*), which depend on the activity of synaptically connected neurons,

$$p^{\mathrm{A}}_{v,k} = \alpha_{v,k} x_k \tag{2a}$$

$$p^{\mathrm{I}}_{v,k} = \iota_{v,k} (1 - x_k) . \tag{2b}$$

In (2), $x_k(t)$ and (1-$x_k(t)$) are relative to the activation and inactivation levels of neuron k, respectively. The parameters $\alpha_{v,k}$ and $\iota_{v,k}$ denote the activation and inactivation propensities of neuron v in response to neuron k. The subscripts v,k indicate that these quantities describe directed interactions from neuron k to neuron v; specifically, $p^{A}_{v,k}$ represents the activation (superscript A) payoff of neuron v based on the activation state of neuron k, and similarly, $p^{I}_{v,k}$ represents the inactivation (superscript I) payoff contribution under the same directional relationship. When both parameters are positive, an emulative relationship is established between v and k: if k is active, the activation payoff for v increases while the inactivation payoff decreases, making v more likely to activate as well. Conversely, when α and ι are negative, a non-emulative relationship arises between v and k. As in [18], we assume that for any ordered pair of neurons (v,k), the propensities $\alpha_{v,k}$ and $\iota_{v,k}$ are either both equal to -1 or both equal to $+1$. Equilibria (A,A) and (I,I) will be referred as the emulation strategies, whereas (A,I) and (I,A) will be the non-emulation strategies. Formalizing the problem of generating neuronal activity patterns among synaptically connected neurons through EGT, involves conceptualizing the membrane potential of the vth neuron (x_v) as a player deciding its activation level depending on a payoff. Mathematically, the problem can be formalized as reported in [18]:

$$\dot{x}_v(t) = x_v(t)(1 - x_v(t)) \sum_{k=1}^{N} a_{v,k} \Delta p_{v,k}(t) . \tag{3}$$

In (3), the parameter $a_{v,k}$ describes the influence of the neuron k on neuron v. Additionally, $\Delta p_{v,k}(t)$ quantifies the difference between the activation and inactivation payoffs for neuron v concerning neuron k. This payoff quantifies the reward associated with the vth neuron's decision to activate (A) or remain inactive (I), accounting for variations in the activity levels of the neurons with which it communicates (figure 1). When $\Delta p_{v,k}(t)$ is greater than 0, meaning

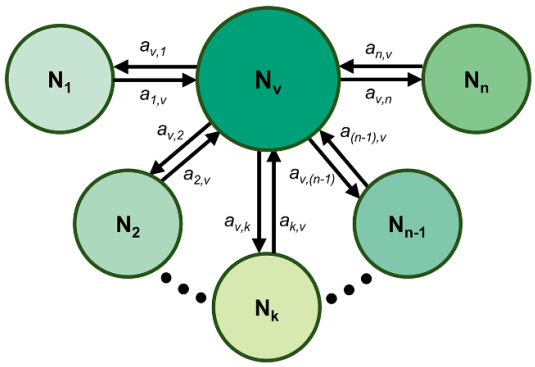

Figure 1. Sketch of the simulated neuronal networks (where neurons are represented by circles) using the evolutionary game theory (EGT) formalism. Each vth neuron can establish emulation relationships (indicated by arrows) between pairs of neurons with an emulation parameter $a_{v,k}$ which takes into account the strength of the interaction.

the payoff for activation exceeds the payoff for inactivation, $x_v(t)$ increases, leading to a higher level of activation. It is worth noting that in (3) two main components can be distinguished: (i) the first is the product of x_v and $(1 - x_v)$, which depends solely on the intrinsic state of the player v (whether it represents a neuron or a brain area); (ii) the second is the summation of payoff terms, weighted by the coefficients $a_{v,k}$, and derived from the contributions of all other players. Since the latter component more effectively captures the influence of a network of players on the vth player, we hypothesized that defining the input current I_v as this summation term from equation (3) would provide a suitable way to integrate the HR and EGT models. Thus, combining the state equations of the HR model (1) with the one of the EGT, we obtained a new set of equations that were simulated (4). This new formulation of the model retains the three original differential equations of the HR neuron, while assigning the variable $I = I(t)$ the summation that captures the payoff values and the coefficients $a_{v,k}$, which are drawn from the domain of EGN.

$$\begin{cases} \dot{x}_v(t) = y_v(t) - x_v^3(t) + b x_v^2(t) - z_v(t) + I_v(t) \\ \dot{y}_v(t) = 1 - 5x_v^2(t) - y_v(t) \\ \dot{z}_v(t) = \mu (s(x_v(t) - x_r) - z_v(t)) \\ I_v(t) = \sum_{k=1}^{N} a_{v,k} \, \Delta p(t)_{v,k} = \sum_{k=1}^{N} a_{v,k} (2x_k - 1) \end{cases} . \tag{4}$$

Since the goal of this work lies in examining how EGT parameters modulate neuronal dynamics, we maintained consistency and prevent potential systematic errors by keeping the HR parameters b, μ, s, and x_r, constant and identical across all neurons in the model as reported in table 1.

Table 1. Parameters of the Hindmarsh–Rose model kept constant in all the simulations.

Hindmarsh–Rose parameters		
Parameter	Spiking dynamics	Bursting dynamics
b	3.0	2.5
μ	0.01	0.01
s	4	4
x_r	−1	−1

The values of these parameters, which are dimensionless, were derived from [26].

2.3. Evaluation of pattern coherence with emulation and non-emulation properties

Emulation and non-emulation represent the emergent properties of EGT. To evaluate whether the patterns generated by the model align with these theoretical principles, we developed a quantitative method based on the successful rate (*SR*) parameter. This metric measures the coherence between the generated patterns and the expected emulation or non-emulation dynamics. Practically, for each generated pattern, we detected the timing of the peaks by means of a hard threshold. We derived a binary activation vector for each neuron where elements are assigned a value of 1 if the sample falls within a spike's lifetime (set at 500 samples), indicating the presence of an action potential; otherwise, they are set to 0 in the absence of activity. The *SR* metric is computed taking into account all implemented strategies, and it is representative of the overall pattern generation across the network. Notably, the computation of the *SR* parameter differs for emulative (5*a*) and non-emulative (5*b*) networks.

$$SR_{\mathrm{em}} = \frac{1}{N_{\mathrm{s}}} \sum_{i=1}^{N_{\mathrm{s}}} \frac{\left(S_i^0 + S_i^1\right)}{S_{\mathrm{tot}}} \tag{5a}$$

$$SR_{\mathrm{non-em}} = \frac{1}{N_{\mathrm{s}}} \sum_{i=1}^{N_{\mathrm{s}}} \frac{\left(S_i^0 + S_i^{01}\right)}{S_{\mathrm{tot}}}. \tag{5b}$$

In (5*a*) and (5*b*), N_{s} is the total number of strategies of the network, which corresponds to all non-zero coefficients $a_{v,k}$, contained in the strategy matrix $A_{v,k}$, while S_{tot} is the total number of samples of the simulations (equal for all generated patterns). S_i^0 denotes the count of samples simultaneously exhibiting a 0 value in both activation vectors of neurons within the ith strategy. Similarly, S_i^1 indicates the number of occurrences where both activation vectors within the ith strategy simultaneously exhibit the value of 1. On the other hand, S_i^{01} represents the number of timestamps where one of the two vectors within the ith strategy contains a 0 while the other contains a 1. In the emulative case (5*a*), we embedded the term S_i^1, as it increases with the simultaneous activity of the two neurons within the ith strategy. Conversely, in the non-emulation scenario (5*b*), we included the term S_i^{01}, which has a higher value the more frequently one neuron's activity tends to coincide with quiescence of the other neuron of the ith strategy. However, the term S_i^0 is included in both (5*a*) and (5*b*), as the simultaneous absence of activity of the two neurons within the ith strategy is compatible with both emulative and non-emulative scenarios. When it is required to quantify the fidelity to the principles of EGT emulation for electrophysiological patterns generated from a non-fully emulative or non-emulative network, the overall *SR* value is given by the average of all SR_i values corresponding to each ith strategy. The *SR* parameter ranges between 0 and 1. The closer this metric gets to 1, the more accurately the generated patterns preserve the principles of emulation and non-emulation characteristic of EGT.

2.4. Estimation method

We first simulated small-scale networks of neurons with connectivity parameters designed to predict different dynamic regimes: AA, II (emulative) and AI, IA (non-emulative). To infer these connectivity parameters from the evolving dynamics of the simulated neuronal populations, we developed a method capable of performing simultaneous state and parameter estimation within linear time-varying systems. The observer was applied to time series data representing the neurons' action potentials, enabling the recovery of the original connectivity parameters set during the simulation. Finally, we assessed whether the recovered estimates were consistent with the EGN-B framework. This methodology was applied by keeping the following assumptions: i) x_v is the sole observable variable for each vth neuron and ii) the parameters inherent to the HR model are known *a priori* and remain constant over time (table 1). To better apply this approach, we now introduce the definitions of w_v (6*a*) and a_v (6*b*).

$$\boldsymbol{w}_v = \begin{bmatrix} x_v \\ y_v \\ z_v \end{bmatrix} \tag{6a}$$

$$\boldsymbol{a}_v = \begin{bmatrix} a_{v1} \\ a_{v2} \\ \vdots \\ a_{vn} \end{bmatrix}. \tag{6b}$$

In (6*a*), $\boldsymbol{w}_v$ denotes a time-varying m-dimensional column vector, where $m = 3$ indicates the number of states within the HR model. Each element of $\boldsymbol{w}_v$ corresponds to one of the state variables in the HR model, specifically representing the state of the vth neuron. On the other hand, a_v is a n-dimensional column vector (6*b*), where n corresponds to the number of neurons defining the network whose electrophysiological behavior is simulated. Each element in the array a_v represents an EGT parameter ($a_{v,k}$, i.e. the weight of the connection that

characterizes the emulation or non-emulation relationship between neuron v and neuron k). Having defined these two quantities (6), we can now rewrite equation (4) in a vectorized form, omitting, for the sake of simplicity, its time dependence:

$$\dot{\boldsymbol{w}}_v = A\boldsymbol{w}_v + \boldsymbol{h}(\boldsymbol{w}_v) + \Xi(\boldsymbol{w})\,\boldsymbol{a}_v. \tag{7}$$

The specific structures of matrices A, $\boldsymbol{h}(\boldsymbol{w}_v)$, and $\Xi(\boldsymbol{w})$ are provided in (8*a*)–(8*c*) as follows:

$$A = \begin{bmatrix} 0 & 1 & -1 \\ 0 & -1 & 0 \\ \mu s & 0 & -\mu \end{bmatrix} \tag{8a}$$

$$\boldsymbol{h}(\boldsymbol{w}_v) = \begin{bmatrix} bx_v^2 - x_v^3 \\ 1 - 5x_v^2 \\ -\mu s x_r \end{bmatrix} \tag{8b}$$

$$\Xi(\boldsymbol{w}) = \begin{bmatrix} 2x_1 - 1 & 2x_2 - 1 & \cdots & 2x_n - 1 \\ 0 & 0 & \cdots & 0 \\ 0 & 0 & \cdots & 0 \end{bmatrix}. \tag{8c}$$

It is worth mentioning that the time-varying matrix $\boldsymbol{h}(\boldsymbol{w}_v)$ contains all non-linear components of the HR dynamics equation. In contrast, the matrix A remains constant over time, and given our assumption that the values of s and μ are uniform across all neurons, both A and $\Xi(\boldsymbol{w})$ matrices remain invariant with respect to the considered neuron. The objective of the following estimation method is to accurately determine all $a_{v,k}$ values, among each pair of vth and kth neurons, assuming only the membrane potential x_v is known. Several studies have addressed the estimation problem, particularly in the context of isolated neuron models. In [28], a global optimization strategy was used to estimate the parameters of single (i.e. not synaptically connected) HR neurons. However, that work does not extend to networks of interconnected neurons and does not consider parameter estimation in the presence of structured interaction terms. Other studies like [29, 30], demonstrated the applicability of adaptive observers in estimating parameters in small HR networks (e.g. two coupled neurons), supporting the viability of observer-based approaches in network settings. These results justify our choice of adaptive observers as a suitable and validated framework for the estimation process. To achieve this, we adjusted the adaptive observer devised in [25, 29] as reported in (9).

$$\begin{cases} \dot{\hat{\boldsymbol{w}}} = A\hat{\boldsymbol{w}}_v + \boldsymbol{h}(\hat{\boldsymbol{w}}_v) + \Xi(\hat{\boldsymbol{w}})\,\hat{\boldsymbol{a}}_v \\ + \left(K + \Xi(\hat{\boldsymbol{w}})\,\Gamma\,\Xi(\hat{\boldsymbol{w}})^T C^T \Sigma\right)\left(\boldsymbol{w}_v^{obs} - C\hat{\boldsymbol{w}}_v\right) \\ \dot{\hat{\boldsymbol{a}}}_v = \Gamma\,\Xi(\hat{\boldsymbol{w}})^T C^T \Sigma\left(\boldsymbol{w}_v^{obs} - C\hat{\boldsymbol{w}}_v\right) \end{cases}. \tag{9}$$

In (9), and $\hat{a}_v$ represent the estimated states and EGT parameters, respectively, for the vth neuron, while $K + \Xi(\boldsymbol{w})\Gamma\Xi(\boldsymbol{w})^T C^T \Sigma$ is the total gain matrix, primarily responsible for stabilizing the estimation process. Examining this latter term, $K \in R^m$ is the gain matrix, $\Gamma \in R^{nxn}$ represents any symmetric positive definite matrix, and $\Xi(\boldsymbol{w}) \in R^{mxn}$ is a matrix containing known signals. Lastly, $\Sigma \in R^{uxu}$ can adopt the structure of any uniformly bounded positive definite matrix, where u denotes the number of outputs in the system, with $u = 1$ in our specific case. Here, w_v^{obs} designates the sole observable state among the three constituting the dynamics of the vth neuron. The identification of the observable state with x_v, i.e. the membrane potential, dictates that $C = [1,0,0]$, making $w_v^{\text{obs}} - C\,\hat{w}_v$ the error incurred during the estimation process. Supplementary material (section S1) reports the assumptions and conditions essential for ensuring the observer's convergence.

To quantify the goodness of the estimation parameters ($\hat{a}_{v,k}$) to approximate the true ones ($a_{v,k}$), we employed the relative squared error (*RSE*) metric in the following formulation:

$$RSE = \frac{\sum_{v=1}^{n}\sum_{k=1}^{n}\left(a_{v,k} - \hat{a}_{v,k}^r\right)^2}{\sum_{v=1}^{n}\sum_{k=1}^{n} a_{v,k}^2}. \tag{10}$$

The superscript r in the parameter $\hat{a}_{v,k}^r$ indicates that the temporal evolution of the corresponding estimation parameter $\hat{a}_{v,k}$ has reached a steady-state value. In the presented simulations, for each pair (v, k), the $\hat{a}_{v,k}^r$ value, defined as the average of the $a_{v,k}$ parameters corresponding to the last decade of the whole simulation time, was computed. This approach reduces the sensitivity in the computation of the value to small periodic variations in the parameter $\hat{a}_{v,k}$. A thorough exploration of the rationale behind the choice of the *RSE* as metric to assess the accuracy of the $\hat{a}_{v,k}$ parameters in estimating the true ones is reported in the supplementary material (section S2).

2.5. Small-world index

The degree of small-worldness of simulated networks was measured by computing the Small-World Index (SWI) [31]. It is defined by the ratio of the average clustering coefficient of the simulated network C_{sim} to the mean shortest path length of the simulated network L_{sim}, multiplied by the ratio of the mean shortest path length of a random network L_{rnd} to the average clustering coefficient of the random network C_{rnd}:

$$\text{SWI} = \frac{C_{\text{sim}}}{L_{\text{sim}}}\,\frac{L_{\text{rnd}}}{C_{\text{rnd}}}. \tag{11}$$

The clustering coefficient C_i and the mean shortest path length L are defined as:

$$C_i = \frac{E}{\frac{k_i(k_i-1)}{2}} \tag{12a}$$

$$L = \frac{2}{n(n-1)}\sum_{i\neq j}\text{dist}(i,j). \tag{12b}$$

In (12*a*) E and k_i are the number of edges between neighbors of i, and the ith node's degree, respectively,

while in (12*b*) n is the number of nodes within the network, and dist(i,j) is the shortest distance between nodes i and j. Since the computation of C_{sim} and L_{sim} requires a binary matrix as input, where entries corresponding to a functional emulative connection between nodes are set to 1 and the remaining to 0, we followed this pipeline: (i) starting from the strategy matrix $A_{v,k}$, we applied the model to obtain the electrophysiological patterns of all neurons; (ii) for each pair of generated electrophysiological patterns, we computed the SR_{em}, thus obtaining *a posteriori* matrix of values between 0 and 1, where the closer a value is to 1, the stronger is the functional emulative connection between the corresponding nodes; (iii) this matrix was arbitrarily thresholded, with all values above 0.7 considered indicative of an emulative strategy and set to 1, while the remaining values were set to 0; (iv) the resulting binary matrix was then used to compute the SWI. It is worth noting that using the posteriori binary matrix (based on emulative *SR* values between nodes) for the SWI computation is a better alternative than using the predetermined strategy matrix $A_{v,k}$. Indeed, using the *a priori* strategy matrix by preserving positive $a_{v,k}$ values and setting them to 1 while zeroing the remaining ones would not provide a valid reference for which relationships were actually emulative. As previously mentioned, while strategies with a positive $a_{v,k}$ coefficient are emulative, it is possible that an emulative strategy might also exist between nodes with a null $a_{v,k}$ coefficient. A simple example is a 3×3 $A_{v,k}$ matrix where emulation is only imposed between neurons 1 and 2, and neurons 1 and 3. Even though no strategy is imposed between neurons 2 and 3 ($a_{2,3} = 0$), it is easy to intuit that an emulative tendency effectively exists between these two nodes. The clustering coefficient and path length values calculated from the simulated functional network are normalized with respect to expected values from equivalent random networks, i.e. networks with the same number of nodes and links. A network is considered to exhibit small-world characteristics when SWI > 1 [31].

2.6. Statistics

To assess whether the Small World Index (SWI) distributions obtained from simulated networks followed the same trend as those derived from experimental data, a Kruskal–Wallis non-parametric test was performed. A significance threshold of 0.05 was adopted; a p-value greater than this threshold was interpreted as evidence of no statistically significant difference between experimental and simulated distributions.

2.7. Simulation protocol

The length of each presented simulation was set to $T = 5000$. The simulation time does not have a direct equivalent in seconds. The HR model primarily operates within the framework of mathematical simulations, where time is represented in terms of timestamps or samples rather than real-world seconds [32, 33]. Simulations were carried out in continuous time using MATLAB's ODE commands, specifically employing the 'ode45' integration algorithm. The solver dynamically adjusted the time step based on a relative tolerance of 10^{-6} and an absolute tolerance of 10^{-9}, as set in the odeset options. To ensure consistency in the output, solutions were interpolated at equispaced time points defined in a user-specified time vector with a time step of $\Delta t = 0.01$. Given that the total simulation time was $T = 5000$, this resulted in $5{\cdot}10^5$ samples per simulated dynamic.

3. Results

In the following sections, we presented the results achieved by the simulations of diverse activity patterns obtained using the HR model described in (4) with the principles of the EGT. Simulations were presented by increasing the complexity of the network, starting from the simplest conditions involving only two neurons, up to more intricate configurations with a higher number of neurons and connections in order to better mimic realistic experimental configurations. In addition, we proved how the estimation method is able to successfully set the EGT parameters ($a_{v,k}$). Finally, we showcased the ability of the estimation process, evaluating its performance as the number of neurons of the simulated networks increases.

3.1. Pattern generation between two coupled neurons

To simulate all the patterns arising from the interaction of two coupled neurons interacting according to the considered paradigm (4), we thoroughly took into account the key factors influencing their membrane potentials: the intrinsic dynamics, characterized by either spiking or bursting patterns, and the appearance of either emulative or non-emulative behavior at the synaptic level. To simulate the former, we set the parameter b of (4) at 2.5 for bursting dynamics and 3 for spiking dynamics (table 1). For the synaptic interaction, we set $a_{v,k} > 0$ and $a_{v,k} < 0$, for the emulative and non-emulative behaviors respectively [18]. We initially explored the following four network configurations: (i) emulative bursting (figure 2(a)), (ii) non-emulative bursting (figure 2(b)), (iii) emulative spiking (figure 2(c)), and (iv) non-emulative spiking (figure 2(d)). For each neuron of these configurations, we simulated the temporal behavior of the state variables x, y, and z, of the HR model (4). Specifically, x describes the membrane potential, while y and z represent the fast and slow kinetics of the ion channels, respectively. For the properties of the HR model, all these state variables are dimensionless. This initial set of simulations aimed at proving

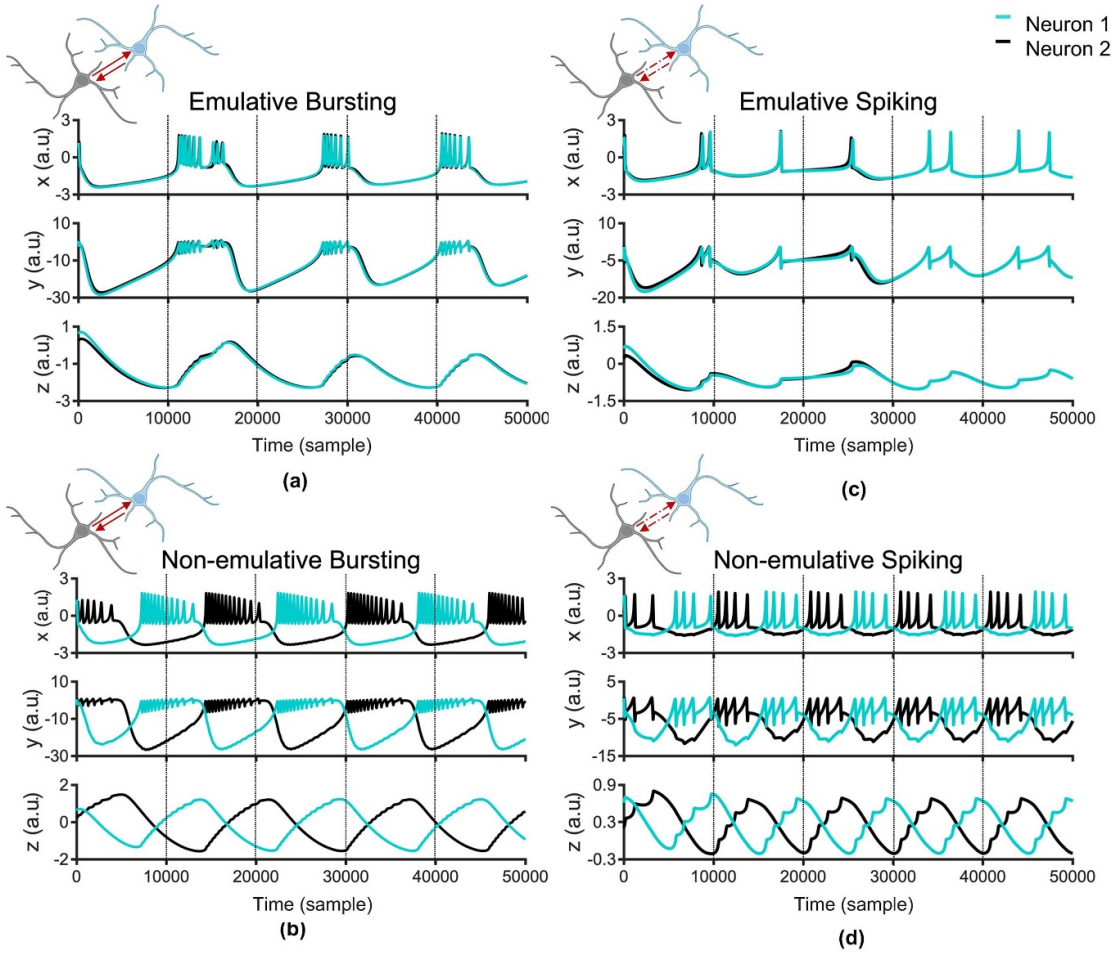

Figure 2. Simulated activity patterns of two interconnected neurons (black and light blue). For each neuron, we simulated the temporal evolution of the x, y, and z state variables of the Hindmarsh–Rose (HR) model (1), representing the membrane potential, the fast and slow ion channel kinetics, respectively. By setting the parameter b (table 1) of the HR model, bursting (a), (b) or spiking dynamics (c), (d) can be simulated. In the emulative bursting (a) or spiking (c) configurations, both $a_{1,2}$ and $a_{2,1}$ parameters of (4) were set to 0.15, while in the non-emulative bursting (b) and spiking (d), $a_{1,2}$ and $a_{2,1}$ were set to −0.15. In all the presented simulations, the self-emulation values ($a_{1,1}$ and $a_{2,2}$) were set to zero, ensuring that the dynamics of each neuron is only influenced by the activity of the other one.

that the HR model keeps the capability to generate diverse dynamics spanning from spiking to bursting patterns, while adhering to the fundamental principles of EGT. These results suggested how the interplay observed among brain areas described in [18], can also be found at micro-circuit level by embedding the EGN principles into the parameter I (the input current of the HR model) of (1). Specifically, in both bursting and spiking activity patterns, the setting of emulative (positive $a_{v,k}$ coefficients) results in nearly temporal alignment of activity patterns between the two neurons (figures 2(a)–(c)). Conversely, when non-emulative (negative) $a_{v,k}$ coefficients are set, the periods of activity in one neuron match the periods of quiescence of the other one, and vice versa (figures 2(b)–(d)). To quantitatively confirm the consistency between the EGT-imposed strategies and the emerging patterns, we computed the *SR* for all four configurations, obtaining values equal to or greater than 0.99 in every condition. Furthermore, to demonstrate the model-free nature of the formalism proposed in this work, we replicated the two-neuron simulations for the same four configurations using three different neuronal models: Izhikevich [34], Adaptive Exponential (AdEx) [35], and Hodgkin–Huxley (HH) [36] (supplementary material S3). The resulting *SR* values further supported the generalizability of our approach: in the case of Izhikevich neurons, *SR* values were consistently greater than or equal to 0.96; for AdEx neurons, all four configurations yielded *SR* values equal to 1; and for the HH model, which was simulated only in the spiking configuration, both emulative and non-emulative cases resulted in *SR* values equal to 1. These results quantitatively confirm the compatibility between the EGT-imposed strategies and the emergent activity patterns across neuron models, highlighting the model-free applicability of the method.

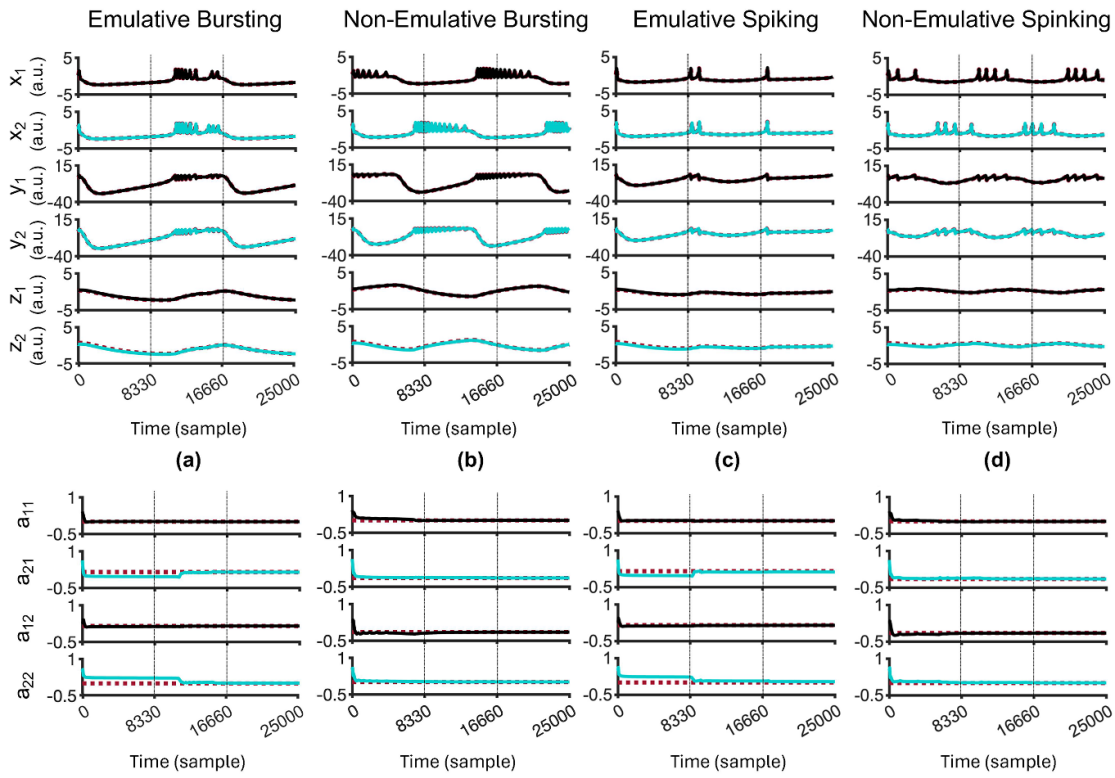

Figure 3. Temporal patterns resulting from the states (a), (b), (c), and (d) and parameters (e), (f), (g), and (h) estimation method applied on the model. The considered networks are made up of two neurons in the emulative bursting (a), and (e), non-emulative bursting (b), and (f), emulative spiking (c), and (g), and non-emulative spiking (d), and (h) configurations. The estimating trends are shown in black for neuron 1 and in light blue for neuron 2, while the model-generated true ones are denoted by a red dotted line.

3.2. Parameters value estimation of patterns generated by two coupled neurons

In this section, the estimation method described in section 2.4 was applied to derive $a_{v,k}$ parameters values solely from the observation of the membrane potential of the neurons in the simulated network. The initial validation of this method involves its ability to estimate the vectors $\boldsymbol{a}_1$ and $\boldsymbol{a}_2$ in the four fundamental scenarios when only two neurons are coupled (i.e. emulative spiking, emulative bursting, non-emulative spiking and non-emulative bursting). In this context, the observable variables are restricted to the membrane potentials x_1 and x_2. Employing adaptive observers implemented by (9), we proved successful in estimating the EGT values in the four considered configurations (figure 3). Qualitatively, the estimation process effectively captures the dynamics of all states *x*, *y*, and *z* of the HR model (1) for both neurons in each of the four considered configurations (figures 3(a)–(d)). The close alignment between the estimated and actual state trajectories further demonstrates the effectiveness of the adaptive observers. Reliable results (in terms of accuracy) were also achieved for the estimation of the EGT parameters $a_{v,k}$ (figures 3(e)–(h)) since the estimating trend quickly converges as well. The quantitative validation of the effectiveness of adaptive observers in simultaneously estimating the state and parameters (based on the sole observation of one of the three variables comprising the model's state) was performed by computing the *RSE* across all the considered configurations (section 3.1), as reported in table 2.

Table 2. Relative squared error (*RSE*) derived from the estimation of EGT parameters.

	RSE values	
	Emulative interaction	Non-emulative interaction
Spiking dynamics	$1.90\ 10^{-3}$	$6.11\ 10^{-6}$
Bursting dynamics	$2.97\ 10^{-5}$	$5.28\ 10^{-5}$

These results demonstrated better performances of the estimation method in the case of bursting dynamics, where the *RSE* values are $2.97{\cdot}10^{-5}$ (emulative) and $5.28{\cdot}10^{-5}$ (non-emulative), regardless of the type of synaptic interaction. In contrast, the estimation outcomes for spiking dynamics vary in a wider range depending on whether synaptic emulation ($1.90{\cdot}10^{-3}$) or non-emulation ($6.11{\cdot}10^{-6}$) is present. The best performance of the estimation method corresponds to the non- emulative spiking configuration; however, even the highest *RSE* value (i.e. the worst case), obtained in the emulative spiking case, still indicates good reliability of the method.

3.3. Design of the strategy matrix $A_{v,k}$: preserving small-world properties in the simulated networks

In this section, we first described the structure of the strategy matrix $A_{v,k}$ and we demonstrated how it tends to generate networks that preserve the typical topological properties, like the small-worldness, of real neuronal networks. To evaluate the scalability of the developed model in more intricate and complex networks, we simulated the following conditions: (i) not all neurons of the network exhibit identical dynamics, whether it is spiking or bursting behavior, (ii) not all neurons play the same strategy, whether they emulate or do not emulate the membrane potential of other neurons of the network. Our model allows for the arbitrary setting of which neurons exhibit purely bursting or spiking dynamics by fixing the percentages of pure spiking (p_{spike}) and pure bursting (p_{burst}) neurons. By tailoring the value of $a_{v,k}$ parameters contained in the strategy matrix $A_{v,k}$, the model allows the fine-tuning of the relationships between neurons, whether emulative or non-emulative, allowing each strategy present in the network to be arbitrarily set. This ensures control over the balance between spiking and bursting activities and allows for direct manipulation of the percentages of emulative (p_{em}) and non-emulative ($p_{\text{non-em}}$) strategies characterizing the neuronal interactions within the simulated network. For the sake of simplicity, the simulated networks described in this section adhere to the following conditions:

(i) Strategy matrices $A_{v,k}$ are symmetric ($a_{v,k} = a_{k,v}$ $\forall v,k$), which implies that if neuron v does (not) emulate neuron k, then neuron k will also do (not) emulate neuron v;
(ii) the self-emulation or self-nonemulation relationships are neglected ($a_{v,v} = 0$ $\forall v$);
(iii) each strategy matrix $A_{v,k}$ is organized as follows: a strategy is established between the first two neurons; the third neuron exhibits a single strategy towards one of the previous two neurons (which of the first two neurons the strategy is applied to is randomly chosen), then, iteratively, the ith neuron will establish a strategy with only one of the previous i-1 neurons, and so on until reaching the total number of neurons in the network. Hence, the resulting network contains n-1 strategies. Afterwards, p_{em} and $p_{\text{non-em}}$ are set: the specific strategies designated as emulative or non-emulative are randomly chosen, yet maintaining the predetermined percentages. In this way, the

non-zero elements of the matrix $A_{v,k}$ correspond to the strategies imposed in the network. However, the zero values in the same matrix do not imply the exclusion of emulativity or non-emulativity between the corresponding neurons. They simply do not impose any specific strategy. This means that two neurons, v and k, whose strategy is formalized by a coefficient $a_{v,k} = 0$, may exhibit either emulativity or non-emulativity depending on how the strategies imposed (whose $a_{v,k}$ coefficient is non-zero) impact the emergent dynamics of the network. The generative algorithm of matrix $A_{v,k}$ ensures that instances of incompatibility are avoided (e.g. configurations where a neuron must simultaneously emulate two others with conflicting, non-emulative strategies). Furthermore, we demonstrated that the design of the strategy matrix according to this algorithm, allows mimicking the typical small-world properties of large-scale neuronal assemblies across three different balance conditions between emulative and non-emulative components: 50:50, 70:30, and 30:70. For each balance condition, $n = 5$ networks of 60 neurons were generated by varying the randomness seed, which altered the establishment of various strategies among the nodes. To quantify the small-world properties of the simulated networks, we computed their SWI (cf, section 2.5). For all three conditions of balance between emulation and non-emulation, the median of the distributions is higher than 1 (figure 4), confirming the ability of these networks to preserve small-world properties. Additionally, we computed the SWI for $n = 10$ *in vitro* cortical networks (supplementary section S4). To show that the distributions of the *in silico* networks follow the same trend of the experimental networks, a Kruskal–Wallis nonparametric test, which provides a single global p-value across all groups, was performed. No statistically significant difference was found ($p = 0.34$).

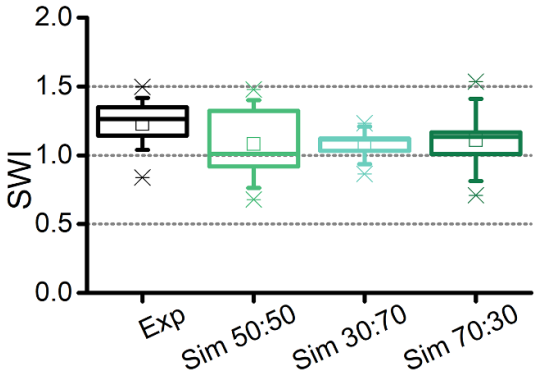

Figure 4. Comparison of the Small World Index (SWI) distributions evaluated from n = 5 *in vitro* cortical multi-electrode array (MEA) recordings (black) with simulated networks displaying an emulation-to-non-emulation ratio of 50:50 (light green), 30:70 (aquamarine), and 70:30 (dark green). A Kruskal–Wallis test, revealed no significant differences among the distributions (p = 0.34). The dashed black lines identify SWI values of 0.5, 1, and 1.5.

3.4. Generation of complex network patterns

In this section, we show how the strategy matrices $A_{v,k}$ can be used to simulate complex networks. We firstly exploited the algorithm to generate the matrix $A_{v,k}$ to simulate a five-neuron network (figure 5(a)),

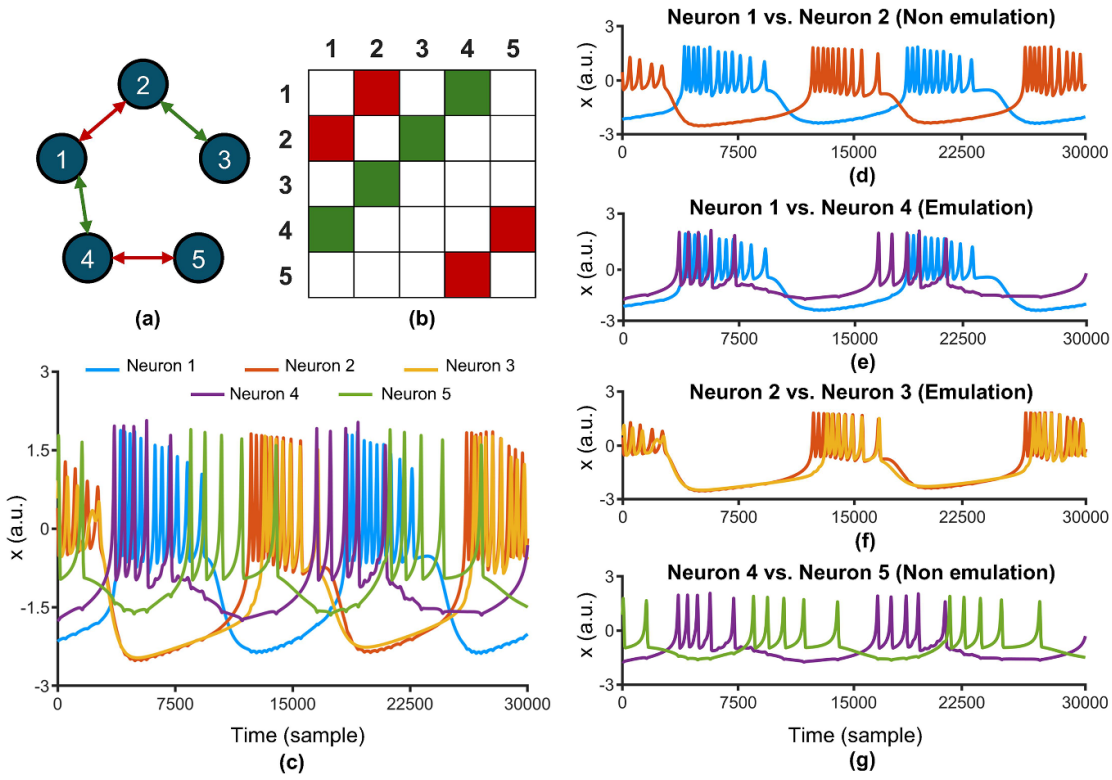

Figure 5. Simulated electrophysiological dynamics of a 5-neurons network. (a) Schematic representation of the network, where neurons are illustrated as circles, and the arrows between neurons represent emulative (green) and non-emulative strategies (red). (b) Color code representation of the connectivity matrix $A_{v,k}$, where the $a_{v,k}$ values of 0 (no interactions), 0.15 (emulative interaction), and −0.15 (non-emulative interaction) are encoded by white, green, and red, respectively. (c) Electrophysiological patterns generated by the five neurons (color coded) of the network. Membrane potentials of 1st and 2nd (d), 1st and 4th (e), 2nd and 3rd (f), and 4th and 5th (g) neurons are represented. In panels (e) and (f), an emulative behavior is observed between neurons 1 and 4, and neurons 2 and 3, as their electrophysiological activity phases are temporally aligned. Conversely, in panels (d) and (g), between neurons 1 and 2, and neurons 4 and 5, when one neuron exhibits electrophysiological activity the other remains inactive, highlighting a non-emulative interaction.

where neurons 1, 2, and 3 display a purely bursting activity, while neurons 4 and 5 exhibit spiking activity. The obtained strategy matrix $A_{v,k}$ (figure 5(b)) is configured such that a non-emulative dynamic exists both between the first two bursting neurons (figure 5(d)), and spiking neurons (figure 5(g)). On the other hand, concerning the two remaining relationships within the network, emulative strategies are played both between neurons 1 and 4 (figure 5(e)), and between the bursting neurons 2 and 3 (figure 5(f)). Qualitatively, the electrophysiological patterns of the individual neuron pairs are strongly consistent with strategies set by the $A_{v,k}$ matrix. In emulative cases, periods of activity are temporally aligned (figures 5(e) and (f)), while in non-emulative ones, the neuron's active periods predominantly coincide with the other neuron's quiescent periods (figures 5(d)–(g)). From a quantitative point of view, the achieved *SR* value results equal to 0.90, indicating the model's efficacy in preserving the EGT principles. Although a five-neuron network is still an example of small-scale neuronal network that does not fully replicate the electrophysiological behavior of a real biological neuronal network, it allows to clearly understand the emulation and non-emulation strategies among individual neurons. To prove the robustness and reliability of the proposed approach, we scaled up to a larger network made up of 20 neurons (10 spiking and 10 bursting neurons). We set balanced emulative and non-emulative strategies (emulation-to-non-emulation ratio of 50:50). Since the number of neurons is even, the number of strategies must necessarily be odd, so this case includes 10 emulative strategies and 9 non-emulative ones. From a qualitative perspective, it is evident that the emulative and non-emulative relationships set in the strategy matrix (figure 6(a)) are consistent with the actual electrophysiological behavior: the raster plot shown in figure 6(b) clearly highlights the percentages of bursting (figure 6(b), *top*) and spiking neurons (figure 6(b), *bottom*). Quantitatively, the model's ability to generate electrophysiological patterns consistent with the strategies imposed in the $A_{v,k}$ matrix is indicated by an *SR* value of 0.91, confirming the model's performance even in the case of a larger network.

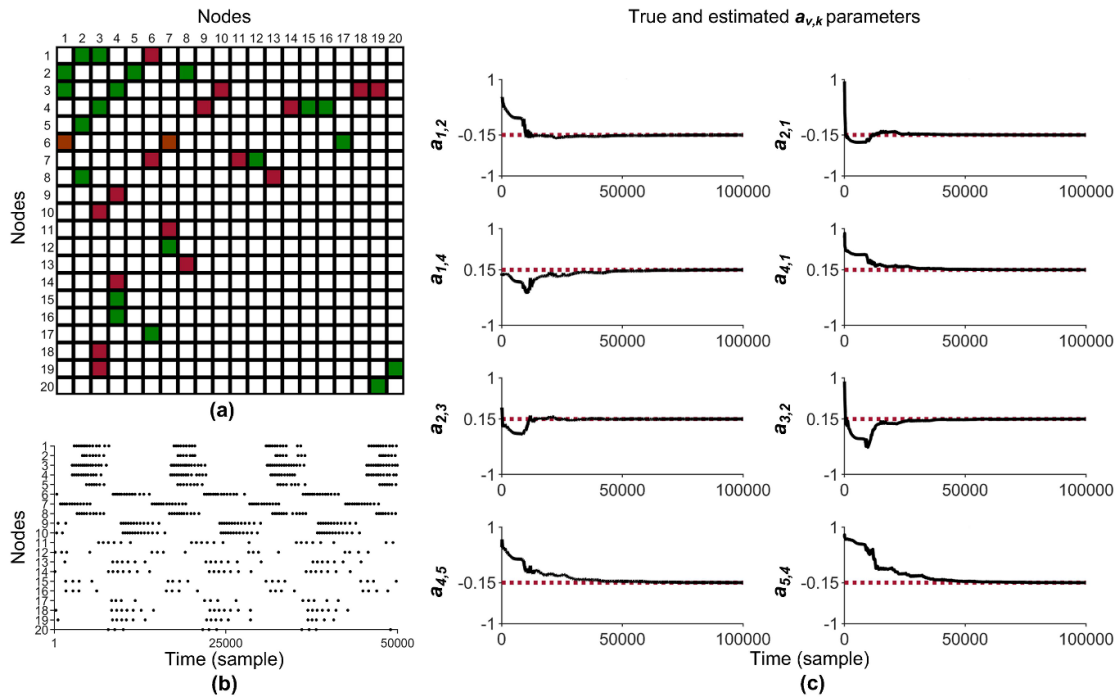

Figure 6. (a) Color code representation of the connectivity matrix $A_{v,k}$ of a 20-neurons network where the $a_{v,k}$ values of 0 (no interactions), 0.15 (emulative interaction), and −0.15 (non-emulative interaction) are encoded by white, green, and red, respectively. (b) Raster plot illustrating the sample activation time of the simulated action potentials generated by the model (each line represents the activity of a neuron). (c) Temporal evolution of adaptive observers estimating evolutionary game theory (EGT) parameters, resulting from the estimation method (9) applied to the model. These temporal trends refer to the eight parameters imposed in the $A_{v,k}$ matrix of the 5-neuron network (figure 5(b)). Each pair of parameters $a_{v,k}$, $a_{k,v}$ (i.e. each row in the figure) corresponds to a strategy. The estimating trends are shown in black, while the model-generated true ones are denoted by a red dotted line.

3.5. Parameter estimation of complex network patterns

In section 3.2, we demonstrated the capability of the estimation method to infer EGT parameters in the simple case of two interacting neurons displaying the same intrinsic pattern of activity (i.e. spiking or bursting), playing the same strategy (i.e. emulative or non-emulative). In this section, we showed that the parameter process estimation remains efficient when applied to larger networks involving both bursting and spiking neurons, playing emulative and non-emulative strategies. In this case, the only observable variable is the intracellular membrane potential x_ν of each νth network node. We tested the goodness of the estimation method to networks made up of 5 and 20 neurons. It is worth noting that the number of $a_{v,k}$ parameters increases with the square of the number of neurons involved in the network. This led to a drastic increase in the complexity of the adaptive observer equation. For clarity, in the case of the 5-neuron network (figure 6(c)), we only showed the estimating trend of the parameters corresponding to the strategies imposed by the strategy matrix (i.e. all non-zero $a_{v,k}$). However, the same type of convergence was observed for the estimation of all other 17 parameters (supplementary section S5). From a quantitative point of view, the performances of the estimation method for the EGT parameters were evaluated in both the 5-neuron and 20-neuron networks (supplementary sections S5 and S6), yielding *RSE* values of 4.57 10^{-6} and 10 10^{-4}, respectively.

3.6. Assessing model scalability as the network size increases

In this section, we showed the effectiveness of both the proposed model (4) and the estimation method (9) in network configurations closer to experimental conditions. To analyze the model's performance, we assessed the ability of the generated patterns to maintain the principles of emulation and non-emulation by computing the *SR* trend as a function of the number of neurons in the network. On the other hand, to demonstrate the efficiency of the estimation method, we evaluated how the *RSE* changed as a function of the number of neurons defining the network. Practically, we simulated and tested networks consisting of a minimum of 5 up to a maximum of 35 neurons (step of 5 neurons), using absolute values of the $a_{v,k}$ parameters of 0.05, 0.1, 0.15, and 0.2. We considered different absolute values for the $a_{v,k}$ coefficients to verify the robustness of the model and the estimation method, ensuring that both the *SR* and *RSE* metrics remained consistent and did not indicate performance degradation as the absolute values of $a_{v,k}$

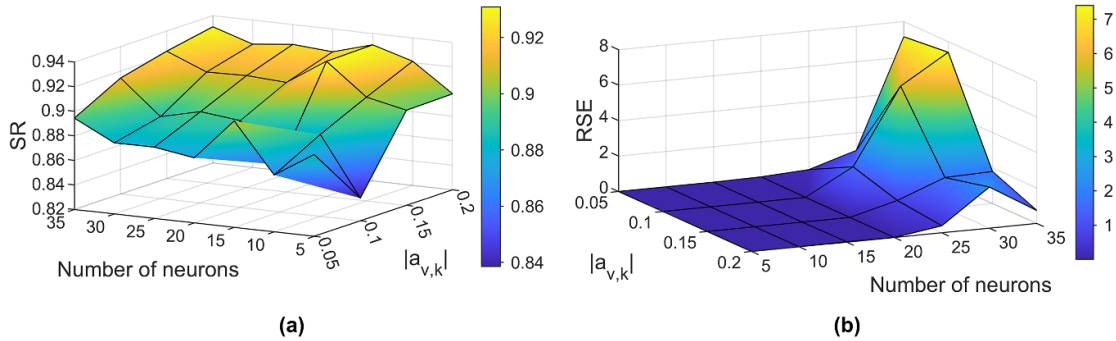

Figure 7. Trends of (a) successful rate (SR) and (b) relative squared error (RSE), as functions of the absolute value of the $a_{v,k}$ parameters and the number of neurons of the simulated network.

varied. The *SR* values indicated strong performance in the entire explored parameter space (figure 7(a)).

The lowest *SR* value observed is 0.84, corresponding to a network of 5 neurons interacting according to $a_{v,k}$ parameters with an absolute value of 0.1. For each pair of neurons and $a_{v,k}$ parameters, the *SR* values are always above 0.8 revealing the coherence between the strategies set with the $A_{v,k}$ matrix and the actual patterns generated. There was no marked decrease in performance by increasing the number of neurons. In addition, the pattern generation appeared more consistent with the imposed strategies as the absolute value of the EGT parameters increased. Concerning the performance of the parameter estimation method, the *RSE* values suggested that the accuracy of the estimation is not optimal throughout the entire parameter space explored (figure 7(b)). In particular, when the network size exceeds 20 neurons, the *RSE* values tend to increase, indicating a worsening of the adaptive observers accuracy in the estimation of the $a_{v,k}$ parameters. Similarly, for each absolute value of the $a_{v,k}$ coefficients, a marked decrease in estimating accuracy emerges as the dimensionality of the simulated network increases. This was due to the convergence of the estimation method to values of $a_{v,k}$ different from the one that actually generated the electrophysiological pattern being considered. In this case, when the number of neurons increases, it becomes more likely that the same configuration of network electrophysiological patterns can be obtained with a greater number of EGT parameter combinations. This penalizes the estimation process, as high *RSE* values may be obtained even when the system converges to values different from the true parameters but still generating *x*, *y*, and *z* states trends equal to the real ones.

3.7. Model versatility: from intracellular to extracellular signals

The EGT inspired model (4) successfully simulates the states of the HR neuron, considering the intracellular membrane potentials of each neuron as players executing a strategy. In addition, the estimation method of (9) relies solely on the observation of the intracellular membrane potential to derive the EGT parameters. However, the proposed approach can be generalized to other kind of signals related to neuronal activity, like the ones achieved by extracellular recordings [37]. In this scenario, the players are not the intracellular membrane potentials (state x of the HR neuron, (4)) but the extracellular ones (defined as v_{ext}).

To generalize the model to account for extracellular membrane potentials, we introduced an electrical representation of the interface between the neuronal membrane and the recording electrode in (4) using the approach devised in [37], where the input-output relationship between the intracellular and extracellular membrane potentials is described by a differential equation (cf, supplementary materials section S7 for their derivation and references therein). Exploiting the approach devised in [37], we can write the input-output relationship between x and v_{ext} as given by (13):

$$\dot{v}_{\text{ext}} = -\alpha v_{\text{ext}} - \beta \dot{x}. \tag{13}$$

The parameters α and β are constant and their values depend on the capacitive and resistive effects present at the electrode-electrolyte interface [37]. For simplicity, both α and β have been set to 1. Substituting $\dot{x}$ with the first equation of the HR model reported in the (4) yields:

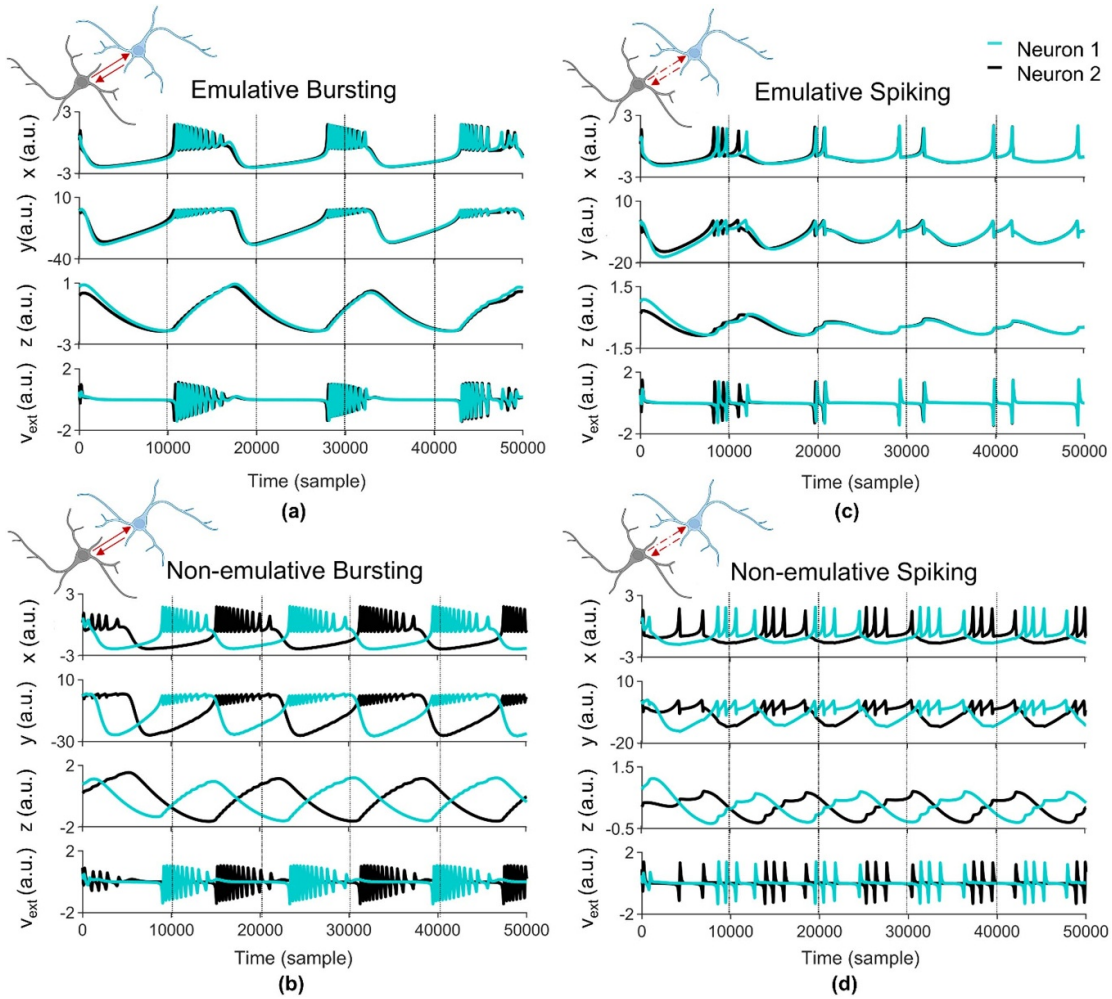

Figure 8. Simulation of the 4th dimensional model reported in equation (15) with two interconnected neurons (light blue and black). For each neuron, we simulated the temporal behavior of the four state variables: x, y, z, and v_{ext}, representing the membrane potential, the fast ion channel kinetics, the slow ion channel kinetics, and the extracellular potential, respectively. The model exhibits either bursting (a), (b) or spiking dynamics (c), (d). For the emulative interactions (a, c), both $a_{1,2}$ and $a_{2,1}$ parameters were set to 0.1. For the non-emulative interactions (b), (d), the same parameters were set to −0.1. The self-emulation values ($a_{1,1}$ and $a_{2,2}$) were kept at zero.

$$\dot{v}_{\text{ext}} = -\alpha v_{\text{ext}} - \beta\left(y - x^3 + bx^2 - z + \sum_{k=1}^{N} a_{v,k}\,(2x_k - 1)\right). \tag{14}$$

Inserting (14) into the model (7) yields:

$$\begin{bmatrix} \dot{x} \\ \dot{y} \\ \dot{z} \\ \dot{v}_{\text{ext}} \end{bmatrix} = \begin{bmatrix} 0 & 1 & -1 & 0 \\ 0 & -1 & 0 & 0 \\ \mu s & 0 & -\mu & 0 \\ 0 & -\beta & \beta & -\alpha \end{bmatrix} \begin{bmatrix} x \\ y \\ z \\ v_{\text{ext}} \end{bmatrix} + \begin{bmatrix} bx^2 - x^3 \\ 1 - 5x^2 \\ -\mu s x_r \\ -\beta\left(bx - x^3\right) \end{bmatrix} + \begin{bmatrix} 2x_1 - 1 & \dots & 2x_n - 1 \\ 0 & \dots & 0 \\ 0 & \dots & 0 \\ \beta\,(1 - 2x_1) & \dots & \beta\,(1 - 2x_n) \end{bmatrix} \begin{bmatrix} a_{v1} \\ a_{v2} \\ \vdots \\ a_{vn} \end{bmatrix}. \tag{15}$$

The application of the model reported in (15) successfully reproduced the extracellular potential dynamics corresponding to the same configurations considered in figure 2. In the case of emulative synaptic interaction, the bursting dynamics exhibited an *SR* of 0.95 (figure 8(a)), while the spiking dynamics showed an *SR* of 0.98 (figure 8(c)). Conversely, in the non-emulative case, both bursting (figure 8(b)) and spiking dynamics (figure 8(d)) resulted in an *SR* of 1, indicating optimal model performance in terms of pattern generation. This result confirmed the maintenance of both the characteristics of the HR model (distinction between bursting and spiking dynamics) and the emergent properties of EGT (emulation and non-emulation among players), even when the simulated patterns represent extracellular rather than intracellular potentials. Finally, we also proved the application of the proposed estimation method (9) to the model of (15). In this case, in order to infer the parameters $a_{v,k}$ from which the electrophysiological

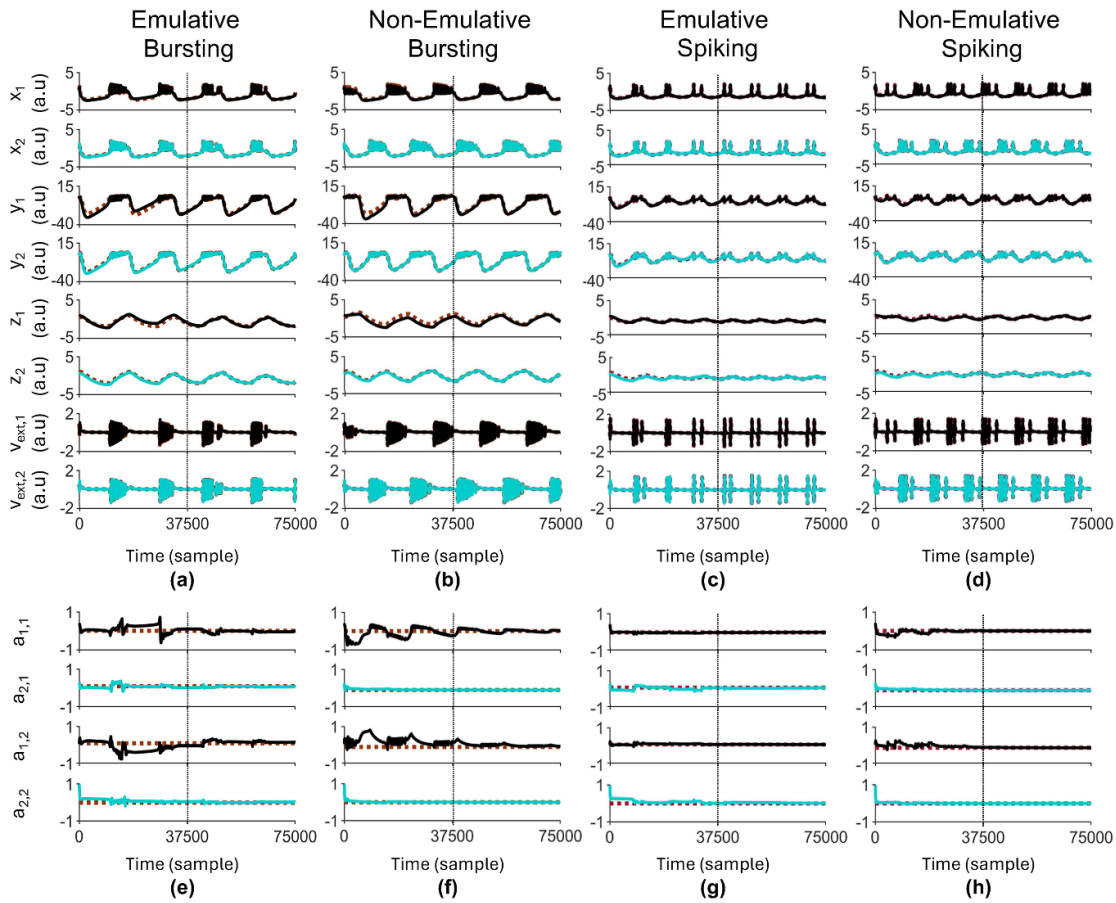

Figure 9. Temporal patterns resulting from the state (a), (b), (c), and (d) and parameter (e), (f), (g), and (h) estimation method applied on (15). The networks examined consist of two neurons arranged in four different configurations: emulative bursting (a) and (e), non-emulative bursting (b) and (f), emulative spiking (c) and (g), and non-emulative spiking (d) and (h). Estimating trends for neurons 1 and 2 are shown in black and light blue, respectively. The actual trends produced by the model (15) are represented by a red dotted line.

Table 3. Relative squared error (*RSE*) derived from the estimation of EGT parameters, considering the extracellular potential as the observable state.

	RSE values	
	Emulative interaction	Non-emulative interaction
Spiking dynamics	$3.39\ 10^{-4}$	$4.61\ 10^{-5}$
Bursting dynamics	$6.00\ 10^{-4}$	$6.42\ 10^{-5}$

patterns originate, the only observable variables are v_{ext1} and v_{ext2}, rather than x_1 and x_2. Despite this change, the estimating trends of both $a_{v,k}$ parameters, and the states of the system successfully converge (figure 9). The *RSE* values, reported in table 3, confirm the reliability of the estimation method.

These results demonstrated a better performance of the estimation process in cases where the synaptic interaction is non-emulative, with *RSE* values in the order of 10^{-5}, regardless of whether the dynamics are spiking or bursting. Conversely, in the case of emulative interaction, both spiking and bursting dynamics show *RSE* values that are larger by one order of magnitude. However, even in the case of emulative strategy, an *RSE* in the order of 10^{-4} still indicates good reliability of the method. Overall, these results indicated that both the model and the estimation method can be easily adapted and applied to different scenarios beyond those for which they were originally designed.

4. Discussion

In computational neuroscience, *in silico* models are crucial to disentangling the mechanisms underlying experimentally observed electrophysiological patterns. Different mathematical formalisms provide different perspectives allowing the analysis of particular features of the neuronal dynamics. In this study, we demonstrated how EGT can be successfully applied to model neuronal interactions at the single cell and synaptic level. Specifically, the computational models presented in this work (Hidmarsh–Rose, Adaptive Exponential Integrate-and-Fire, Izhikevich, Hodgkin and Huxley) allow for the generation of electrophysiological patterns whose interactions are formalized by the 'game' played among network nodes.

EGT was already utilized in various domains, including modeling the interplay between fMRI signals of different brain regions [18]. Both Madeo *et al*, work and our study employ EGT to model neuronal interactions. Our approach focuses on the microscale, capturing synaptic-level interactions between individual neurons. This approach can be seen as an alternative method to model synaptic interactions, typically described by means of biophysical or phenomenological approaches [38]. A limit of the current implementation of the EGT formalism in modeling synaptic transmission is its intrinsic time-invariance: no long-term time constants (due to short/long term mechanisms) were taken into account. The time-invariant nature of the present EGT formalism does not account for the dynamic evolution of strategies over time, which is critical in modeling progressive changes especially in pathological conditions that alter the connectivity balance. In contrast, Madeo *et al* used EGT to describe functional connectivity at the macroscale, modeling interactions between large-scale brain regions based on fMRI resonance patterns. This shift in scale implies that while Madeo *et al* captured interregional coordination, our approach focuses on the local mechanisms shaping neuronal dynamics. The successful application of this method across networks of different sizes and independently of the kind of mechanisms used to model the single neuron dynamics underscores the scalability of the model within the tested range.

Additionally, to support the goodness of the developed approach and its application to experimental applications, we proved how the simulation of these strategies recreates a connectivity pathway that retains the small-world properties observed in *in vitro* cortical networks coupled to MEAs [39].

The estimation process of the EGN parameters was achieved by developing a method based on the observation of simulated electrophysiological activity patterns. We obtained it using adaptive observers, which allow estimating both the state and the parameters of the model from the sole observation of a part of the overall state of the HR neuron, namely the membrane potential. Earlier studies addressed parameter estimation mainly in isolated HR neurons, such as the global optimization approach of [28], which did not extend to networks or structured interactions. In contrast, works like [29, 30] confirmed that adaptive observers can operate effectively even in small coupled HR networks, supporting their suitability for our network-level estimation task. This estimation method extends the capabilities of the proposed model, as it allows it to be used not only as a mathematical tool for generating electrophysiological patterns, but also as a computational approach able to derive EGT strategies present in a neural network. Our findings indicate the efficiency of both the model and the estimation method, even when applied to medium-scale neuronal networks (figures 6 and 7). In fact, after thoroughly examining the main types of interactions that can occur between two connected neurons according to the proposed computational framework (figure 2), we simulated networks where different types of strategies between players (i.e. the intracellular membrane potential of neurons) coexist within the same network (figure 5).

Finally, to increase the versatility of the proposed model, we introduced a new differential equation into the HR model to describe the extracellular membrane potential. We showed (figure 9) that the estimation process of EGT parameter remains effective even when the only observable variable is the extracellular membrane potential. This add-on to the model increases its applicability in experimental cases where extracellular recordings are taken from a neuronal network.

In perspective, an important implication of the approach presented in this work lies in its potential for experimental data analysis. The ability to estimate game-theoretic parameters from intra- or extracellular dynamics opens the possibility of using these parameters as discriminative markers to compare different experimental models (and/or conditions). The mathematical properties of EGT parameters derived from various electrophysiological recordings could be investigated to determine whether specific neuronal types (e.g. neurons from cortex or hippocampus), or structural properties (e.g. modularity, three-dimensionality, or more complex connectivity schemes [1]), influence the dynamics captured by the EGT framework. These 'games' between neurons or neuronal groups may reflect underlying biological features that differ between experimental models or experimental conditions, like physiological vs pathological conditions. In impaired conditions, EGT-based models may help to identify disruptions/alterations in neuronal 'games' associated with disorders, or neurodegenerative diseases, where synaptic connectivity and plasticity are often impaired [40]. These parameters could serve as computational biomarkers, offering a novel framework for comparing disease models or assessing the impact of pharmacological interventions on network-level dynamics.

Data availability statement

The data that support the findings of this study are openly available at the following URL/DOI: https://doi.org/10.5281/zenodo.17483181.

Supplementary Analyses available at https://doi.org/10.1088/1741-2552/ae1dad/data1.

Acknowledgment

This work was supported by #NEXTGENERATIONEU (NGEU) and funded by the Ministry of University and Research (MUR), National Recovery and

Resilience Plan (NRRP), project RAISE—Robotics and AI for Socio-economic Empowerment.

Author contributions

Fabio Poggio 0000-0002-7354-5314
Data curation (equal), Formal analysis (equal), Methodology (lead), Software (lead), Writing – original draft (equal), Writing – review & editing (equal)

Martina Brofiga 0000-0003-2993-0597
Data curation (equal), Formal analysis (equal), Supervision (equal), Visualization (equal), Writing – original draft (equal)

Cecilia De Vicariis 0000-0001-7200-0892
Investigation (equal), Writing – original draft (equal)

Vittorio Sanguineti 0000-0001-8746-3136
Conceptualization (equal), Formal analysis (equal), Writing – original draft (equal)

Paolo Massobrio 0000-0001-8335-3407
Conceptualization (equal), Formal analysis (equal), Funding acquisition (equal), Project administration (lead), Resources (equal), Supervision (lead), Writing – original draft (equal), Writing – review & editing (equal)

References

[1] Brofiga M, Pisano M, Raiteri R and Massobrio P 2021 On the road to the brain-on-a-chip: a review on strategies, methods, and applications *J. Neural Eng.* **18** 041005
[2] Ballanyi K and Ruangkittisakul A 2008 Brain Slices *Encyclopedia of Neuroscience* eds Binder M D, Hirokawa N and Windhorst U (Springer) pp 483–90
[3] Foley K E 2017 Organoids: a better *in vitro* model *Nat. Methods* **14** 559–62
[4] Sporns O 2003 Graph theory methods for the analysis of neural connectivity patterns *Neuroscience Databases: A Practical Guide* (Springer) pp 171–85
[5] Rolls E T 2023 Neuronal network models *Brain Computations and Connectivity* (Oxford University Press) (https://doi.org/10.1093/oso/9780198887911.005.0002)
[6] Aamir S A, Müller P, Kriener L, Kiene G, Schemmel J and Meier K 2017 From LIF to AdEx neuron models: accelerated analog 65 nm CMOS implementation *2017 IEEE Biomedical Circuits and Systems Conf., BioCAS 2017—Proc.* (https://doi.org/10.1109/BIOCAS.2017.8325167)
[7] Hindmarsh J L and Rose R M 1984 A model of neuronal bursting using three coupled first order differential equations *Proc. R. Soc. B* **221** 1222
[8] Nelson M and Rinzel J 1998 The Hodgkin—Huxley model *The Book of GENESIS* (Springer) (https://doi.org/10.1007/978-1-4612-1634-6_4)
[9] Gasparinatou M M, Matzakos N and Vlamos P 2023 Spiking neural networks and mathematical models *Adv. Exp. Med. Biol.* **1424**
[10] Bullmore E and Sporns O 2009 Complex brain networks: graph theoretical analysis of structural and functional systems *Nat. Rev. Neurosci.* **10** 186–98
[11] Rubinov M, Kötter R, Hagmann P and Sporns O 2009 Brain connectivity toolbox: a collection of complex network measurements and brain connectivity datasets *NeuroImage* **47** S169
[12] Li J, Abbas H, Ang D S, Ali A and Ju X 2023 Emerging memristive artificial neuron and synapse devices for the neuromorphic electronics era *Nanoscale Horiz.* **8** 1456–84
[13] Osborne M J and Rubinstein A 2023 Strategic games *Models in Microeconomic Theory* (Open Book) (https://doi.org/10.11647/obp.0362.15)
[14] Sanfey A G, Loewenstein G, McClure S M and Cohen J D 2006 Neuroeconomics: cross-currents in research on decision-making *Trends Cogn. Sci.* **10** 108–16
[15] De Mesquita B B 2006 Game theory, political economy, and the evolving study of war and peace *Am. Polit. Sci. Rev.* **100** 637–42
[16] Leimar O and McNamara J M 2023 Game theory in biology: 50 years and onwards *Phil. Trans. R. Soc. B* **378** 20210509
[17] De Vicariis C, Chackochan V T and Sanguineti V 2024 Game theory and partner representation in joint action: toward a computational theory of joint agency *Phenom. Cogn. Sci.* **23** 599–628
[18] Madeo D, Talarico A, Pascual-Leone A, Mocenni C and Santarnecchi E 2017 An evolutionary game theory model of spontaneous brain functioning *Sci. Rep.* **7** 1–11
[19] Hammerstein P and Selten R 1994 Game theory and evolutionary biology *Handbook of game theory with economic applications* vol 2 (Elsevier) ch 28, pp 929–93
[20] Hofbauer J and Sigmund K 2003 game dynamics *Bull. Am. Math. Soc.* **40** 479–519
[21] Jackson M O and Zenou Y 2015 Games on networks *Handbook of Game Theory with Economic Applications* (Open Book) (https://doi.org/10.1016/B978-0-444-53766-9.00003-3)
[22] Madeo D and Mocenni C 2015 Game interactions and dynamics on networked populations *IEEE Trans. Autom. Contr.* **60** 1801–10
[23] De Blasi S, Ciba M, Bahmer A and Thielemann C 2019 Total spiking probability edges: a cross-correlation based method for effective connectivity estimation of cortical spiking neurons *J. Neurosci. Methods* **312** 169–81
[24] Friston K, Moran R and Seth A K 2013 Analysing connectivity with Granger causality and dynamic causal modelling *Curr. Opin. Neurobiol.* **23** 172–78
[25] Zhang Q 2002 Adaptive observer for multiple-input-multiple-output (MIMO) linear time-varying systems *IEEE Trans. Automat. Contr.* **47** 525–9
[26] Storace M, Linaro D and De Lange E 2008 The Hindmarsh-Rose neuron model: bifurcation analysis and piecewise-linear approximations *Chaos* **18** 033128
[27] Chen D, Li J, Zeng W and He J 2023 Topology identification and dynamical pattern recognition for Hindmarsh–Rose neuron model via deterministic learning *Cogn. Neurodyn.* **17** 203–20
[28] De Lange E and Hasler M 2008 Predicting single spikes and spike patterns with the Hindmarsh-Rose model *Biol. Cybern.* **99** 349–60
[29] Mukae J, Totoki Y, Suemitsu H and Matsuo T 2011 Parameter and input estimation in Hindmarsh-Rose neuron by adaptive observer *2011 IEEE/SICE Int. Symp. on System Integration, SII 2011* (https://doi.org/10.1109/SII.2011.6147601)
[30] Fradkov A L, Kovalchukov A and Andrievsky B 2022 Parameter estimation for Hindmarsh–Rose neurons *Electronics* **11** 885
[31] Humphries M D, Gurney K and Sporns O 2008 Network 'small-world-ness': a quantitative method for determining canonical network equivalence *PLoS One* **3** e0002051
[32] Cai J, Bao H, Xu Q, Hua Z and Bao B 2021 Smooth nonlinear fitting scheme for analog multiplierless implementation of Hindmarsh–Rose neuron model *Nonlinear Dyn.* **104** 4379–89

[33] Kovalchukov A and Fradkov A L 2022 Speed-gradient approach to Hindmarsh-Rose model identification based on membrane potential measurements *Proc.—6th Scientific School "Dynamics of Complex Networks and Their Applications", DCNA 2022* (https://doi.org/10.1109/DCNA56428.2022.9923232)
[34] Izhikevich E M 2003 Simple model of spiking neurons *IEEE Trans. Neural Netw.* **14** 1569–72
[35] Brette R and Gerstner W 2005 Adaptive exponential integrate-and-fire model as an effective description of neuronal activity *J. Neurophysiol.* **94** 3637–42
[36] Hodgkin A L and Huxley A F 1990 A quantitative description of membrane current and its application to conduction and excitation in nerve *Bull. Math. Biol.* **52** 25–71
[37] Massobrio P, Massobrio G and Martinoia S 2007 Multi-program approach for simulating recorded extracellular signals generated by neurons coupled to microelectrode arrays *Neurocomputing* **70** 2467–76
[38] Destexhe A, Mainen Z F and Sejnowski T J 1998 Kinetic models of synaptic transmission *Methods in Neuronal Modeling* (The MIT Press)
[39] Napoli A, Xie J and Obeid I 2014 Understanding the temporal evolution of neuronal connectivity in cultured networks using statistical analysis *BMC Neurosci.* **15** 17
[40] Dejanovic B, Sheng M and Hanson J E 2024 Targeting synapse function and loss for treatment of neurodegenerative diseases *Nat. Rev. Drug Discov.* **23** 23–42